

Comparative Analysis of k -essence and Quintessence Scalar Field Models: A Data Analysis Approach

Saddam Hussain,^{*} Sarath Nelleri,[†] and Kaushik Bhattacharya[‡]

Department of Physics, Indian Institute of Technology Kanpur, Kalyanpur 208016, India

We perform a comparative analysis of quintessence and k -essence scalar field models in the data analysis perspective. We study the quintessence field with an exponential potential and the k -essence field with an inverse square potential in the present work. Before delving into data analysis, we provide a brief perspective on dynamical evolution on both of the models and obtain the stability constraints on the model parameters. We adopt Bayesian inference procedure to estimate the model parameters that best-fit the data. A comprehensive analysis utilizing Observational Hubble data (OHD) and Pantheon+ compilation of Type Ia supernovae (SNIa) shows that k -essence model fits the data slightly better than the quintessence model while the evidence of these models in comparison with the Λ CDM model is weak. The value of the Hubble constant predicted by both the models is in close agreement with the value obtained by the Planck2018 collaboration assuming the Λ CDM model.

I. INTRODUCTION

Initially, the observation on Type Ia supernovae [1, 2], subsequent independent observations from the Cosmic Microwave Background (CMB), gravitational lensing, large-scale structure, and Baryonic Acoustic Oscillations (BAO) [3–8], indicated the existence of an exotic energy component dubbed dark energy, responsible for the accelerating expansion of the universe. The simplest and widely accepted model that accounts for this observation is Λ CDM where Λ represents the cosmological constant and CDM refers to cold dark matter. However, it poses challenges such as fine tuning problem, cosmic coincidence, Hubble tension among others. The fine-tuning problem refers to a profound disparity of approximately 120 orders of magnitude between the observed value ($\sim 10^{-47}\text{GeV}^4$) and the theoretically predicted value ($\sim 10^{74}\text{GeV}^4$) of the cosmological constant (Λ), assuming it represents the vacuum energy density. The cosmic coincidence problem puzzles over why the densities of dark energy and dark matter appear to be nearly equal in the present epoch [9–16]. The tension problem in cosmology arises from the statistically significant (4σ to 6σ) discrepancy between the cosmological parameters predicted by early-time data assuming the concordance Λ CDM model and a wide range of model-independent local measurements of distances and redshifts. For instance, the Hubble constant (H_0) estimated from CMB data by the Planck2018 collaboration is $67.4 \pm 0.5 \text{ km s}^{-1}\text{Mpc}^{-1}$ [17], whereas direct observations of

^{*} mdsaddamh6@gmail.com

[†] sarathn@iitk.ac.in

[‡] kaushikb@iitk.ac.in

Cepheids by the SHOES team report $73.2 \pm 1.3 \text{ km s}^{-1}\text{Mpc}^{-1}$ [18], indicating a tension of approximately $\sim 4.2\sigma$.

Over the past two decades, researchers have explored various alternative scenarios that can mimic the dynamics of Λ CDM. One of the most popular and heavily investigated mechanisms is the introduction of a scalar field. Inspired by particle physics, a quintessence-type field with a potential term can generate sufficient acceleration in the presence of dark matter [19–28]. Although the quintessence field minimally coupled with dark matter fluid can mimic the dynamical aspect of Λ CDM, it also suffers from fine-tuning of the potential parameter. Later, some string-inspired models, namely k -essence fields with non-linear kinetic terms, have been widely studied, as they were claimed to address some of the shortcomings of the above models. Due to the associated non-linear kinetic terms, these fields have been termed non-canonical fields [29–39]. Despite its success in explaining late-time cosmic acceleration, few attempts have been made to test these models against observational data due to the complexity of solving the Hubble equation to obtain an analytical expression for the Hubble parameter.

It is essential to test the k -essence model against observational data to determine its compatibility. To conduct this analysis, we solve the field and Friedmann equations numerically and obtain the Hubble parameter as a function of redshift. To set initial conditions and priors for the model parameters, we perform a dynamical system analysis. Stability techniques in dynamical systems are powerful tools for studying complex models, as they help identify physically viable solutions by examining the existence and nature of critical points, thereby constraining the model parameters [40–47]. To analyze the stability of the critical points, we set up a system of first-order autonomous differential equations. By linearizing these autonomous equations, we construct a Jacobian matrix and obtain the corresponding eigenvalues. If any real part of the eigenvalues vanish, the linearization method is no longer applicable for determining stability in those cases. In such situations, more rigorous mathematical techniques, such as the center manifold theorem, must be utilized.

In this study, we compare the quintessence and k -essence fields, using exponential and inverse power-law type potentials, respectively, against observational Hubble data (OHD) and Pantheon+ datasets. The dynamics of the quintessence field are potential-dependent, and this field has been extensively studied with a wide range of potentials. [48–50]. However, very few studies have been conducted on purely kinetic k -essence, and k -essence with a Lagrangian which is a general function of X and the ϕ where ϕ is the k -essence field and $X = -1/2g^{\mu\nu}\nabla_\mu\phi\nabla_\nu\phi$ [51, 52]. For the first time, we constrain the parameter space of the k -essence field, where the Lagrangian takes the form $\mathcal{L}_\phi = V(\phi)F(X)$ and compare it with the Λ CDM model in the data analysis perspective.

The paper is systematized as follows. In section II, we present quintessence model and its dynamical system analysis. In section III, we analyse the k -essence model in the dynamical system perspective. Data analysis of the quintessence and k -essence models are presented in section IV. Finally, we conclude in section V. The model comparison performed based on the AIC and BIC criteria shows that the k -essence model is slightly better than the quintessence model.

II. THE QUINTESSENCE FIELD

The action describing the quintessence field minimally coupled with the dark matter fluid is given by:

$$S = \int d^4x \sqrt{-g} \left(\frac{R}{2\kappa^2} + \mathcal{L}_\phi(\partial_\mu \phi, \phi) + \mathcal{L}_m \right), \quad (2.1)$$

where,

$$\mathcal{L}_\phi = \left[\epsilon \frac{1}{2} \partial_\mu \phi \partial^\mu \phi - V(\phi) \right]. \quad (2.2)$$

Here, ϵ serves as a switching parameter with values of ± 1 . $\epsilon = +1$ represents the phantom field, while $\epsilon = -1$ represents the normal quintessence field. In our system of units $\kappa^2 = 8\pi G$ where G is Newton's universal gravitational constant.

Variation of the action with respect to ϕ and the metric $g^{\mu\nu}$ yields the field equations and the energy-momentum tensor of the field:

$$\begin{aligned} \epsilon \nabla_\mu (\nabla^\mu \phi) + \frac{dV}{d\phi} &= 0, \\ T_{\mu\nu}^{(\phi)} &= -\epsilon \partial_\mu \phi \partial_\nu \phi + g_{\mu\nu} \left[\frac{\epsilon}{2} \partial_\alpha \phi \partial^\alpha \phi - V(\phi) \right]. \end{aligned} \quad (2.3)$$

The corresponding energy density and pressure are given by:

$$\rho_\phi = -\frac{\epsilon \dot{\phi}^2}{2} + V(\phi), \quad P_\phi = -\frac{\epsilon \dot{\phi}^2}{2} - V(\phi). \quad (2.4)$$

The equation of state of the field is expressed as:

$$\omega_\phi = \frac{-\frac{\epsilon \dot{\phi}^2}{2} - V(\phi)}{-\frac{\epsilon \dot{\phi}^2}{2} + V(\phi)}. \quad (2.5)$$

For the normal field, to achieve cosmic acceleration, it is required that $V(\phi) \gg \dot{\phi}^2/2$. The Friedmann equation for a spatially flat Friedmann-Lemaitre-Robertson-Walker (FLRW) metric, $ds^2 = -dt^2 + a(t)^2 d\vec{x}^2$, is given by

$$\begin{aligned} 3H^2 &= \kappa^2 (\rho_m + \rho_\phi), \\ 2\dot{H} + 3H^2 &= -\kappa^2 (P_m + P_\phi), \end{aligned} \quad (2.6)$$

where $H \equiv \dot{a}/a$ is the Hubble parameter and $a(t)$ is the scale-factor of the expanding universe. Here, ρ_m and ρ_ϕ represent the energy densities of matter and field components, respectively, P_m, P_ϕ denotes the pressure of the respective components. The energy-momentum tensor of both the field and fluid are individually conserved, resulting in the following conservation equations:

$$\begin{aligned} \dot{\rho}_m + 3H(\rho_m + P_m) &= 0, \\ \dot{\rho}_\phi + 3H(\rho_\phi + P_\phi) &= 0. \end{aligned} \quad (2.7)$$

Note that during the late-time epoch, the universe is primarily dominated by pressureless dust and dark energy. Consequently, one can safely neglect the contribution of radiation from the system. Quintessence has been extensively studied with a wide variety of potentials, ranging from power-law types to exponential potentials. In this paper, we will specifically focus on demonstrating the dynamics for an exponential-type potential [23],

$$V(\phi) = V_0 e^{-\lambda\kappa\phi}, \quad (2.8)$$

where V_0 and λ are constants. In the subsequent section, we will set up the dynamical equations within the framework of dynamical system analysis to understand the stability and nature of solutions.

A. Dynamical system for quintessence fields

To understand the dynamics, we begin by constructing the autonomous system of equations through the definition of dimensionless variables as follows:

$$x = \frac{\kappa\dot{\phi}}{\sqrt{6}H}, \quad y = \frac{\kappa\sqrt{V}}{\sqrt{3}H}, \quad \lambda = -\frac{V_{,\phi}}{\kappa V}, \quad \Omega_m = \frac{\kappa^2\rho_m}{3H^2}, \quad \Omega_\phi = \frac{\kappa^2\rho_\phi}{3H^2}. \quad (2.9)$$

These are the standard definitions of the variables commonly adopted in the literature to describe the dynamics of the system. The parameter x is related to the dynamic velocity of the field, while y describes the evolution of the potential. The fractional densities of the fluid and field are represented by (Ω_m, Ω_ϕ) respectively, and λ is related to the slope of the potential. For the exponential potential, λ becomes a constant. A crucial constraint on the system is imposed by the first Friedmann equation Eq. (2.6),

$$1 = \Omega_m + \Omega_\phi, \quad (2.10)$$

where the physically viable solution must adhere to these limits,

$$0 \leq \Omega_m \leq 1, \quad 0 \leq \Omega_\phi \leq 1. \quad (2.11)$$

Here, the field fractional density and effective equation of state (EoS) for the quintessence field ($\epsilon = -1$) is given by:

$$\Omega_\phi = x^2 + y^2, \quad \omega_{\text{eff}} = \frac{P_m + P_\phi}{\rho_m + \rho_\phi} = x^2 - y^2 \quad (2.12)$$

and the second Friedmann equation, Eq. (2.6), can be expressed in terms of dynamical variables as:

$$\frac{2\dot{H}}{3H^2} = -\left(1 + \omega_m\Omega_m + x^2 - y^2\right), \quad (2.13)$$

where ω_m is the EoS in the matter sector. The autonomous system of equations are as follows:

$$\begin{aligned} x' &= \left(\frac{3y^2\lambda}{\sqrt{6}} - 3x\right) + \frac{3}{2}x\left(1 + \omega_m\Omega_m + x^2 - y^2\right), \\ y' &= \frac{-xy\lambda\sqrt{6}}{2} + \frac{3y}{2}\left(1 + \omega_m\Omega_m + x^2 - y^2\right). \end{aligned} \quad (2.14)$$

Points	(x_*, y_*)	Ω_ϕ	Ω_m	ω_{eff}	Eigenvalues (E_1, E_2)
$P_{1,2}$	$(\mp 1, 0)$	1	0	1	$\left(3, 3 - \sqrt{\frac{3}{2}\lambda}\right)$
P_3	$\left(\frac{\sqrt{\frac{3}{2}}}{\lambda}, \frac{\sqrt{\frac{3}{2}}}{\lambda}\right)$	$\frac{3}{\lambda^2}$	$1 - \frac{3}{\lambda^2}$	0	$\left(-\frac{3(\lambda^2 + \sqrt{24\lambda^2 - 7\lambda^4})}{4\lambda^2}, \frac{3\sqrt{24\lambda^2 - 7\lambda^4}}{4\lambda^2} - \frac{3}{4}\right)$
P_4	$\left(\frac{\lambda}{\sqrt{6}}, \sqrt{1 - \frac{\lambda^2}{6}}\right)$	1	0	$\frac{1}{3}(\lambda^2 - 3)$	$\left(\frac{1}{2}(\lambda^2 - 6), \lambda^2 - 3\right)$
P_5	$(0, 0)$	0	1	0	$\left(-\frac{3}{2}, \frac{3}{2}\right)$

TABLE I. The critical points of minimally coupled quintessence field.

Here, prime denote derivative with respect to N , where $dN = Hdt$. Since the autonomous equations of the system depend only on the two variables of the system, the phase space becomes 2D. The dynamics of the matter fluid can be understood using the Friedmann constraint. The autonomous equation (y') is invariant under ($y \mapsto -y$), and has an invariant submanifold at $y = 0$. Consequently, trajectories originating on this plane remain confined to it. The critical points and their eigenvalues are summarized in Tab. [I] by choosing $\omega_m = 0$. As the matter sector is assumed to be made up of dark matter, our assumption implies that the fluid representing dark matter is pressure-less. We use linearization techniques to determine the stability of the critical points by evaluating the Jacobian matrix defined as follows:

$$J_{ij} = \left. \frac{\partial x'_i}{\partial x_j} \right|_{x_*}, \quad (2.15)$$

where $x_i = \{x, y\}$ for $i = 1, 2$. Corresponding to this autonomous system, the Jacobian matrix becomes 2×2 dimensional. To assess stability, we determine the eigenvalues and based on the signature of the real parts of eigenvalues, the point can be categorized as stable, unstable, or saddle. If all the real parts of the eigenvalues are negative (positive), the corresponding point becomes asymptotically stable (unstable). However, for alternating signs, the point is labeled as a saddle.

The points $P_{1,2}$ specify points where the system is kinetically drive. At this points the potential term vanishes and consequently $y = 0$. Near this points the effective EoS is 1. The other point P_5 , where both field parameters vanish, results in fluid density domination over the field. As a consequence, the effective ω_{eff} becomes zero, signifying matter-dominated characteristics. This point always exhibits saddle-type behavior.

The point P_3 is dependent on the model parameter, and the corresponding equation of state is zero, which may signify the matter regime of the universe. However, from the Friedmann constraint, Eq. (2.10), the point becomes nonphysical for $\lambda^2 \leq 3$. The point can only stabilize for $3 \leq \lambda^2 \leq \frac{24}{7}$. Beyond this range, it becomes unstable.

The point P_4 is also model parameter dependent. At this point, the field density dominates over the fluid density and the equation of state becomes λ dependent. For $\lambda^2 = 3$, the point can generate non-relativistic matter type behavior as ω_{eff} vanishes. However, this point can also produce an accelerating solution for $0 < \lambda^2 < 2$. It is clear that if we select the model parameter in this range, the point P_3 becomes non-physical. The point P_4 can stabilize for

$0 \leq \lambda^2 \leq 3$. This shows that at $\lambda = \sqrt{3}$, the quintessence field behaves as a non-accelerating attractor type field.

We assess the dynamics of the entire system in Fig.[1] for the range of $0.001 \leq x_0 \leq 0.2$, $0.7 \leq y_0 \leq 0.95$, $0.0001 \leq \lambda \leq 1.3$ by generating random numbers within this range. Here, the subscript zero denotes the initial conditions at $N = z = 0$. We have also plotted the evolution of the Hubble parameter and distance modulus, μ , against redshift, z , where μ is defined as

$$\mu = 5 \log_{10}(d_L) + 25, \quad (2.16)$$

where the luminosity distance is given by:

$$d_L = c(1+z) \int_0^z \frac{1}{H(z)} dz, \quad (2.17)$$

for the random numbers generated within the parameter ranges specified above. Here, c represents the speed of light expressed in km/s. We compare it with the corresponding observational data including 43 OHD and 1701 Pantheon+ data sets [53, 54].

From this evolution, one can observe that within these ranges, the scalar field density dominates at the current epoch and stabilizes at point P_4 . However, from the Hubble evolution, it can be seen that as the redshift increases ($z > 0.5$), the trajectories tend to deviate from the data points. While the evolution of the distance modulus does not exhibit significant changes. To obtain the best-fit parameter values of these parameters, we will utilize Bayesian statistics as described in Sec. IV, using a similar range.

III. K-ESSENCE FIELD

The action for the k -essence field, minimally coupled with the dark matter fluid, is given by:

$$S = \int d^4x \sqrt{-g} \left(\frac{R}{2\kappa^2} - \mathcal{L}_\phi(X, \phi) + \mathcal{L}_m \right), \quad (3.1)$$

where the k -essence Lagrangian becomes the pressure of the field. The pressure of the k -essence field is assumed to have a particular form as follows:

$$P_\phi = -\mathcal{L}_\phi = V(\phi)F(X). \quad (3.2)$$

Here, $V(\phi)$ represents the potential of the field, and $F(X)$ depends on the kinetic term of the field, where $X = -\frac{1}{2}g^{\mu\nu}\partial_\mu\phi\partial_\nu\phi$. The potential extensively studied corresponding to this particular form of the Lagrangian, which exhibits scaling behavior in the past epoch and tracking behavior in the current epoch, is the inverse square type of potential given by:

$$V(\phi) = \frac{\delta^2}{\kappa^2\phi^2}. \quad (3.3)$$

The kinetic function of the field takes the form:

$$F(X) = -X + X^2. \quad (3.4)$$

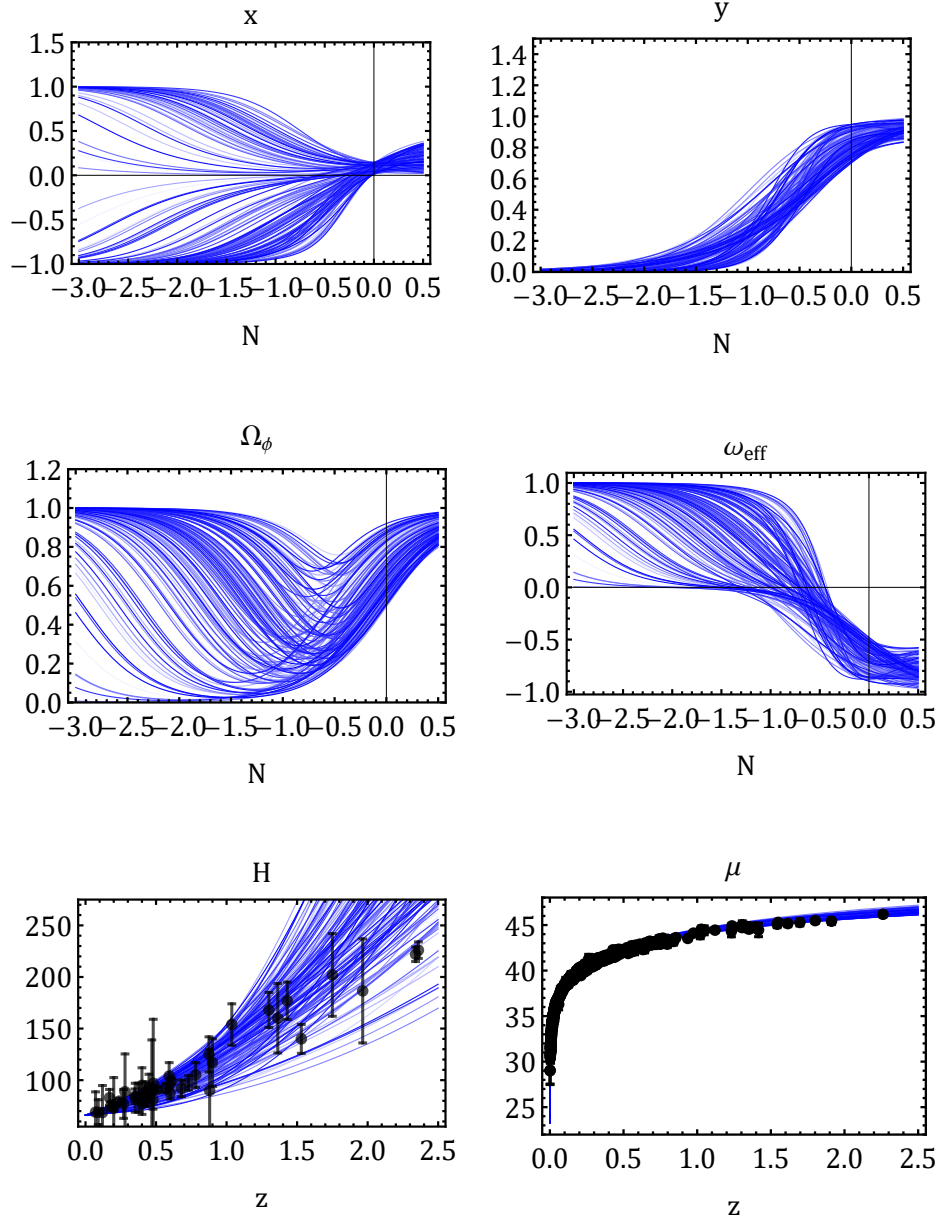


FIG. 1. The evolution of dynamical variables in the quintessence model where $H_0 = 66 \text{ Kms}^{-1}\text{Mpc}^{-1}$.

Upon varying the action of the k -essence with respect to $g^{\mu\nu}$, the stress tensor of the field can be obtained as:

$$T_{\mu\nu}^{(\phi)} = -\mathcal{L}_{,X} (\partial_\mu \phi)(\partial_\nu \phi) - g_{\mu\nu} \mathcal{L}. \quad (3.5)$$

Corresponding to this, the energy density and pressure of the k -essence field can be obtained as follows:

$$\rho_\phi = \mathcal{L} - 2X\mathcal{L}_{,X} \quad \text{and} \quad P_\phi = -\mathcal{L}. \quad (3.6)$$

As the field and fluid components are minimally coupled with gravity, the corresponding individual energy-momentum tensors are conserved:

$$\begin{aligned}\dot{\rho}_m + 3H(\rho_m + P_m) &= 0, \\ \dot{\rho}_\phi + 3H(\rho_\phi + P_\phi) &= 0.\end{aligned}\tag{3.7}$$

Upon varying the action with respect to ϕ , the field equation of motion becomes:

$$(F_{,X} + 2XF_{,XX})\ddot{\phi} + 3HF_{,X}\dot{\phi} + (2XF_{,X} - F)\frac{V_{,\phi}}{V} = 0,\tag{3.8}$$

where the subscript associated with the comma denotes the partial derivative with respect to that quantity. In the spatially flat FLRW metric, the Friedmann equation becomes:

$$3H^2 = \kappa^2(\rho_m + \rho_\phi),\tag{3.9}$$

$$2\dot{H} + 3H^2 = -\kappa^2(\rho_m + \rho_\phi).\tag{3.10}$$

In the subsequent section, we translate these equations into autonomous equations and discuss the stability of the system.

A. Dynamical system stability of k -essence field

After evaluating the background dynamical equations in the aforementioned section, we will analyze the stability of the system by defining a set of dimensionless variables as:

$$x^2 = \frac{\kappa^2 V \dot{\phi}^2}{6H^2}, \quad y^2 = \frac{\kappa^2 V \dot{\phi}^4}{4H^2}, \quad \Omega_m = \frac{\kappa^2 \rho_m}{3H^2}, \quad \lambda = \frac{-V_{,\phi}}{\kappa V^{3/2}}, \quad \Omega_\phi = \frac{\kappa^2 \rho_\phi}{3H^2}.\tag{3.11}$$

We choose the variables corresponding to the field sector such that the Hubble equation takes a similar form to the quintessence field. The primary variables associated with the k -essence field are $x, y > 0$, and are assumed to be positive. Following the Hubble equation Eq. (3.9), the primary variables are (x, y, Ω_m) constrained as:

$$0 \leq \Omega_m = 1 - \Omega_\phi \leq 1, \quad 0 \leq \Omega_\phi \leq 1.\tag{3.12}$$

Here, the field density parameter, Ω_ϕ , and effective equation of state, ω_{eff} , in terms of dynamical variables become:

$$\Omega_\phi = -x^2 + y^2, \quad \omega_{\text{eff}} = \frac{P_m + P_\phi}{\rho_m + \rho_\phi} = \frac{y^2}{3} - x^2.\tag{3.13}$$

The second Friedmann equation can be expressed in terms of dynamical variables as:

$$\frac{\dot{H}}{H^2} = \frac{3}{2} \left(x^2 - \frac{y^2}{3} - 1 \right).\tag{3.14}$$

Points	(x, y)	Ω_ϕ	Ω_m	ω_{eff}	Eigenvalues
P_1	$(0, 1)$	1	0	$1/3$	$(1, 1)$
P_2	$\left(\frac{\sqrt{\frac{3}{\lambda}}}{\lambda}, \frac{3}{\sqrt{2}\lambda}\right)$	$\frac{3}{\lambda^2}$	$1 - \frac{3}{\lambda^2}$	0	$\left(-\frac{3\sqrt{\frac{3}{5}}\sqrt{-\lambda^2(\lambda^2-8)}}{4\lambda^2} - \frac{3}{4}, \frac{3}{20}\left(\frac{\sqrt{15}\sqrt{-\lambda^2(\lambda^2-8)}}{\lambda^2} - 5\right)\right)$
P_3	$\left(-\frac{\sqrt{3\lambda^2+16}+\sqrt{3}\lambda}{2\sqrt{2}}, \frac{1}{2}\sqrt{3\lambda^2+\sqrt{9\lambda^2+48\lambda+12}}\right)$	1	0	$\frac{1}{6}(-3\lambda^2 - \sqrt{9\lambda^2+48\lambda-6})$	Fig. [2a]
P_4	$\left(\frac{\sqrt{3\lambda^2+16}-\sqrt{3}\lambda}{2\sqrt{2}}, \frac{1}{2}\sqrt{3\lambda^2-\sqrt{9\lambda^2+48\lambda+12}}\right)$	1	0	$\frac{1}{6}(-3\lambda^2 + \sqrt{9\lambda^2+48\lambda-6})$	Fig. [2b]
P_5	$(0, 0)$	0	1	0	$(-3/2, -9/2)$

TABLE II. The nature of the critical points of the k -essence field.

To understand the system's dynamics, we take the primary variables and set up the autonomous equations as follows:

$$\begin{aligned}
 x' &= -\frac{\dot{H}}{H^2}x + \frac{1}{2}\sqrt{6}(-\lambda)x^2 + \frac{-\frac{1}{2}\sqrt{6}\lambda x^2 - \frac{2y^2}{x} + 3x + \frac{1}{2}\sqrt{6}\lambda y^2}{\frac{2y^2}{x^2} - 1}, \\
 y' &= -\frac{\dot{H}}{H^2}y + \frac{-\frac{4y^3}{x^2} + \frac{6\lambda y^3}{\sqrt{6}x} - \sqrt{6}\lambda xy + 6y}{\frac{2y^2}{x^2} - 1} + \frac{1}{2}(-\sqrt{6})\lambda xy.
 \end{aligned} \tag{3.15}$$

Here, the time derivative of the dynamical variables is closed and requires no extra variables, as a result, the phase space of the system becomes $2D$. The autonomous equations (x', y') present the invariant submanifold $(x = 0, y = 0)$, hence the trajectories that originate in $x, y > 0$ cannot cross the $x = y = 0$ plane. For the inverse square type potential, the derivative of the potential yields:

$$\lambda = 2/\delta. \tag{3.16}$$

As λ becomes a constant quantity, throughout the analysis, we treat λ as a model parameter instead of δ . Now, we will obtain the critical points associated with the autonomous equations and summarize them in Tab. [II]. The system produces four critical points, and we have considered only those points for which $y > 0$.

- **Point P_1 :** At this point, the field energy density parameter dominates over the fluid energy density parameter and produces an effective equation of state, $\omega_{\text{eff}} = 1/3$, showing radiation-type characteristics. This signifies that the k -essence field can mimic radiation-type behavior in an early epoch of the universe. The eigenvalues at this point yield positive values, indicating unstable behavior.
- **Point P_2 :** At this point, the coordinates become model parameter dependent. Both the field and fluid density parameter are non-zero and dependent on λ . The point can be physically viable for $\lambda^2 \geq 3$. The effective equation of state at this point vanishes, showing pressureless matter fluid-type characteristics. Based on the eigenvalues, the point becomes an attractor point for $\lambda \geq \sqrt{3}$. However, as the point becomes an attractor point in some range of λ , and produces non-accelerating type behavior, it cannot be considered as a viable physical point that describes the late-time phase of the universe.

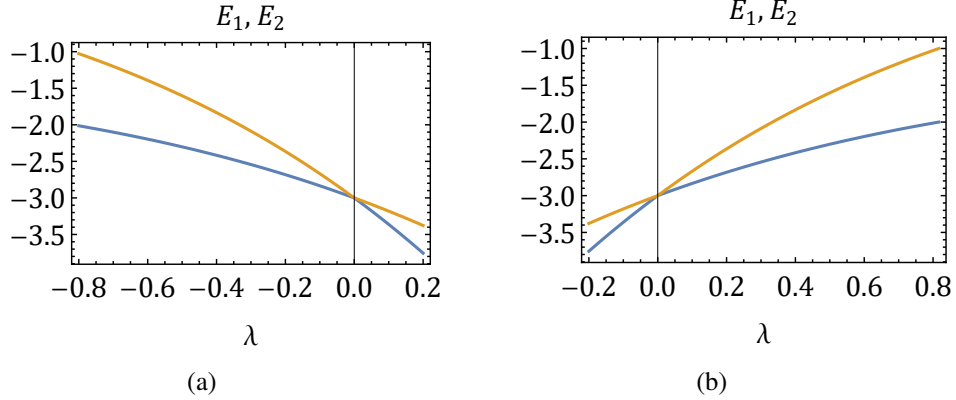


FIG. 2. The evolution of eigenvalues at points $P_{3,4}$ against λ shown in Figs. [2a, 2b] respectively.

- **Point P_3 :** The coordinates are λ dependent, and the field density parameter dominates over the fluid density. The effective EoS, ω_{eff} is λ dependent and produces an accelerating solution, i.e., $-1 \leq \omega_{\text{eff}} \leq -1/3$, for $-0.82 < \lambda < 0$ and a phantom solution, $-1.2 \leq \omega_{\text{eff}} < -1$, for $0 < \lambda < 0.162$. In this range, the real part of the eigenvalues are negative, as shown in Fig. [2a], hence the point becomes stable and shows the late-time behavior of the universe.
- **Point P_4 :** Similar to point P_3 , this point produces acceleration for $0 < \lambda < 0.82$ and phantom-type characteristics for $-0.162 < \lambda < 0$. In this range, the eigenvalues yield negative non-zero real parts, as shown in Fig. [2b], indicating the stable behavior of the point. As this point also features a stable accelerating solution, it is physically viable.
- **Point P_5 :** At this point, both field variables vanish, consequently, the field fractional density becomes zero. The fluid density dominates and the effective equation of state becomes 0, signifying matter-dominated type behavior. However, upon determining the Jacobian matrix, the corresponding eigenvalues yield negative values, making it stable.

Based on the above critical point analysis, we see that the points $P_{3,4}$ produce accelerating and phantom solutions based on the range of λ . However, these two points do not signify the same state of the universe for a particular value of λ , neither do they exist in the same quadrant of the phase space as the coordinates become different. For example, for $\lambda = 0.2$, the coordinates of P_3 become $P_3 = (-1.54, 1.84)$, while $P_4 = (1.30, 1.64)$. One of the major differences can be seen in the sign of the x -coordinate. So, while doing the numerical evolution of the differential equations, as stated earlier, the autonomous equations present a submanifold; consequently, the initial conditions in x , if chosen positive, then the system evolves and stabilizes at P_4 . In terms of phase space, one can say that all the trajectories that have originated in the positive x -axis will remain bound in the first quadrant provided $y > 0$.

The phase space of the system has been plotted for $\lambda = 0.2$ in Fig. [3], where the gray region shows the constraint on field energy density, ($0 \leq \Omega_\phi \leq 1$). The green region shows the accelerating characteristics, ($-1 \leq \omega_{\text{eff}} < -1/3$), when field energy density dominates

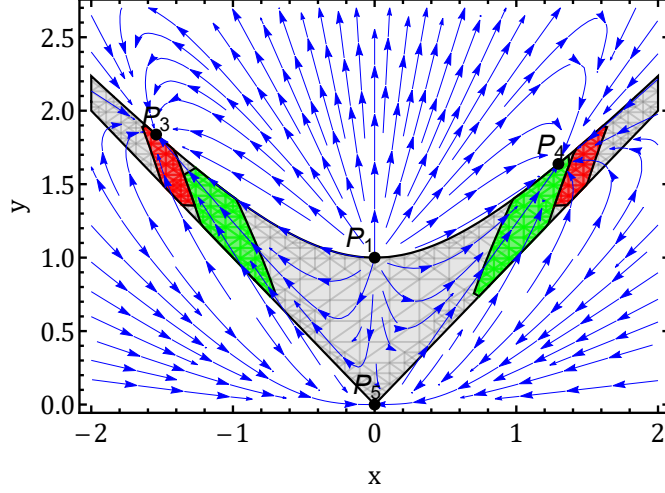


FIG. 3. The phase space of k -essence field for $\lambda = 0.2$.

$0.5 < \Omega_\phi \leq 1$, and the phantom region ($-1.5 < \omega_{\text{eff}} < -1$) is shown in red color. From the phase space, it becomes clear that the trajectories originate from P_1 , which shows radiation-type characteristics, get attracted towards both P_3 and P_4 . Those trajectories whose slopes are positive, $x > 0$ are attracted towards P_4 , while the trajectories with negative slopes, $x < 0$, get attracted towards P_3 . Depending on the choice of λ , either P_3 or P_4 shows accelerating characteristics. There are a few trajectories which are not constrained by the Hubble equation and are not attracted towards $P_{3,4}$; they get attracted to P_5 , which shows an attractor matter regime. Note that point P_2 cannot be considered as a physically viable point, since Ω_m becomes negative for $\lambda^2 < 3$. In Fig. [4], we numerically evolved the system by varying the initial conditions and model parameters in the range of $0.5 \leq x_0 \leq 1.12$, $0.1 \leq \Omega_{m0} \leq 0.32$, $0.001 \leq \lambda \leq 0.4$ by generating random numbers. Here, we have varied Ω_{m0} instead of y_0 , since one can get y_0 using the Hubble constraint equation as,

$$y_0 = \sqrt{1 - \Omega_{m0} + x_0^2}. \quad (3.17)$$

Here, we can see that the initial conditions with $x_0 > 0$ remain positive; hence, the system stabilizes at point P_4 and generates an accelerating solution. We see that although during the late-time epoch, the field energy density dominates, but in the past epoch, the curves corresponding to the Hubble evolution show deviation from the data points. However, there is no substantial difference that can be accounted for in the distance modulus plot. In the subsequent sec. IV, we will conduct statistical analysis to obtain the best fit values of the dynamical variables and model parameters.

IV. DATA ANALYSIS

Our subsequent objective involves performing data analysis to constrain the parameter space of the model. In order to achieve this goal, we need to derive an analytical expression

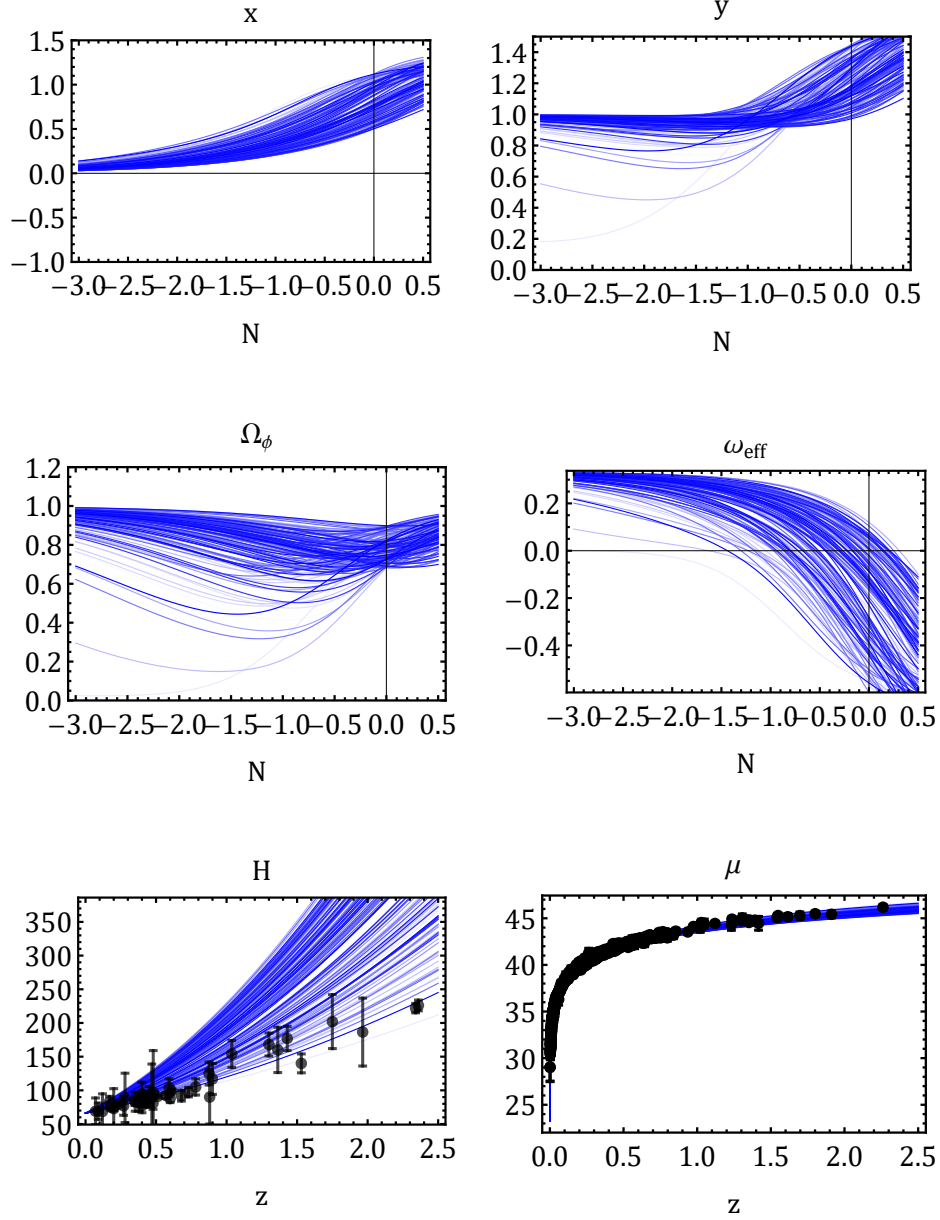


FIG. 4. The evolution of cosmological parameters of the k -essence field for $H_0 = 66 \text{ Km s}^{-1}\text{Mpc}^{-1}$.

for the Hubble parameter as a function of redshift. While this process is straightforward for the Λ CDM model, it poses challenges for quintessence and k -essence models due to the inability to obtain an analytical solution to the Friedmann equation. Therefore, we opted for a dynamical systems approach, solving the coupled differential equations outlined in Eqs. (2.14) and (3.15) to capture the evolution of the Hubble parameter. We utilize the most recent compilation of Type Ia supernovae (SNe Ia) from the pantheon+ dataset [54] along with Observational Hubble data (OHD) [55–57] to obtain the parameters of the model. We adopt

Model	Parameters	priors	OHD	OHD+Pantheon
Λ CDM	H_0	[40, 100]	70.6 ± 1.5	66.8 ± 1.0
	$\Omega_{\Lambda 0}$	[0.5, 0.99]	$0.742^{+0.022}_{-0.019}$	0.675 ± 0.015
	M	[-20, -19]	–	-19.454 ± 0.029
Quintessence	H_0	[40, 100]	$67^{+3.7}_{-2.9}$	66.49 ± 0.98
	x_0	[0, 0.45]	$0.266^{+0.17}_{-0.086}$	$0.311^{+0.036}_{-0.047}$
	y_0	[0.7, 0.92]	$0.810^{+0.059}_{-0.031}$	$0.804^{+0.012}_{-0.018}$
	λ	[0, 1.86]	$1.04^{+0.61}_{-0.41}$	$1.20^{+0.11}_{-0.15}$
	M	[-20, -19]	–	-19.441 ± 0.029
k -essence	H_0	[40, 100]	$66.7^{+3.1}_{-3.7}$	66.41 ± 0.96
	x_0	[0.7, 1.4]	1.122 ± 0.086	1.118 ± 0.023
	Ω_{m0}	[0, 0.9]	$0.191^{+0.11}_{-0.060}$	$0.183^{+0.12}_{-0.054}$
	λ	[-0.2, 19]	0.30 ± 0.23	$0.313^{+0.065}_{-0.055}$
	M	[-20, -19]	–	-19.445 ± 0.028

TABLE III. The 68% confidence of the model parameters.

Model	Data	AIC	BIC
Λ CDM	OHD	27.63	31.15
	Pantheon+OHD	1794.26	1810.66
Quintessence	OHD	30.86	37.91
	Pantheon+OHD	1780.78	1808.10
k -essence	OHD	30.72	37.76
	Pantheon+OHD	1780.73	1808.05

TABLE IV. The statistical quantities corresponding to the data sets.

the Bayesian parameter inference which relies on the Bayes theorem, offering a gratifying description to compute the posterior probability of a particular parameter of interest given the data (D) and model (M). Mathematically, it can be expressed as [58, 59],

$$P(\theta|D, M) = \frac{P(D|\theta, M)P(\theta|M)}{P(D|M)}, \quad (4.1)$$

where $P(\theta|D, M)$ denotes the posterior distribution of the model parameters, $P(D|\theta, M)$ stands for the likelihood, $P(\theta|M)$ is the prior probability distribution. Meanwhile, $P(D|M)$ serves as a normalization factor representing the evidence of the model. Although $P(D|M)$ is insignificant from the parameter estimation, it plays the central role in the model selection. The prior probability incorporate any existing knowledge about the model parameters before the data acquisition. The selection of a prior relies on the expertise of the researcher in the field and quality of judgement. Nevertheless, once the prior is set, iterative application of the Bayes theorem converges to a common posterior [60]. The likelihood is assumed to be Gaussian,

$$P(D|\theta, M) \equiv \exp\left(\frac{-\chi^2(\theta)}{2}\right). \quad (4.2)$$

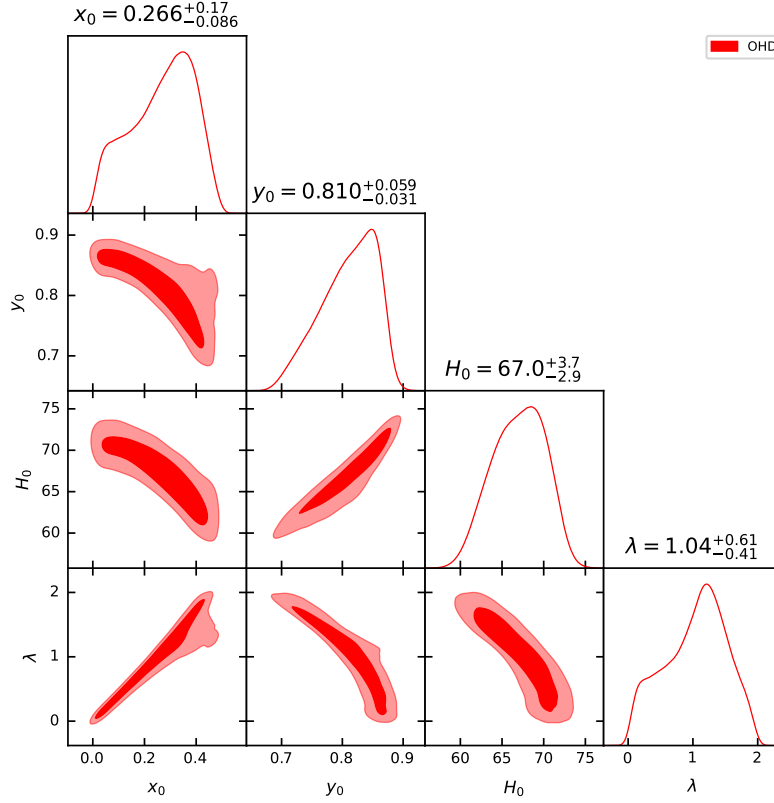


FIG. 5. The Quintessence field is fitted with OHD data.

Here, the χ^2 for the observational Hubble data is computed using the expression

$$\chi_{\text{OHD}}^2 = \sum_k \left[\frac{H_k - H_k(\theta)}{\sigma_k} \right]^2, \quad (4.3)$$

where H_k is the Hubble parameter obtained from the data for the redshift z_k and $H_k(\theta)$ is the corresponding Hubble parameter computed for the model. The OHD data consists of 43 Hubble parameter values obtained in the redshift span $0.07 < z < 2.36$. Among these, 31 data points are obtained from the differential age technique, which are model independent. The remaining 12 data points are derived from the Baryon acoustic oscillation measurement assuming the standard cosmology [53, 56]. The pantheon+ compilation include 1701 SNe Ia light curves of 1550 supernovae observed in the redshift span $0 \leq z \leq 2.3$ [54]. The observable in case of SNe Ia is the apparent magnitude which is computed using the expression,

$$m(z) = 5 \log_{10} \left[\frac{d_L(z)}{\text{Mpc}} \right] + M + 25, \quad (4.4)$$

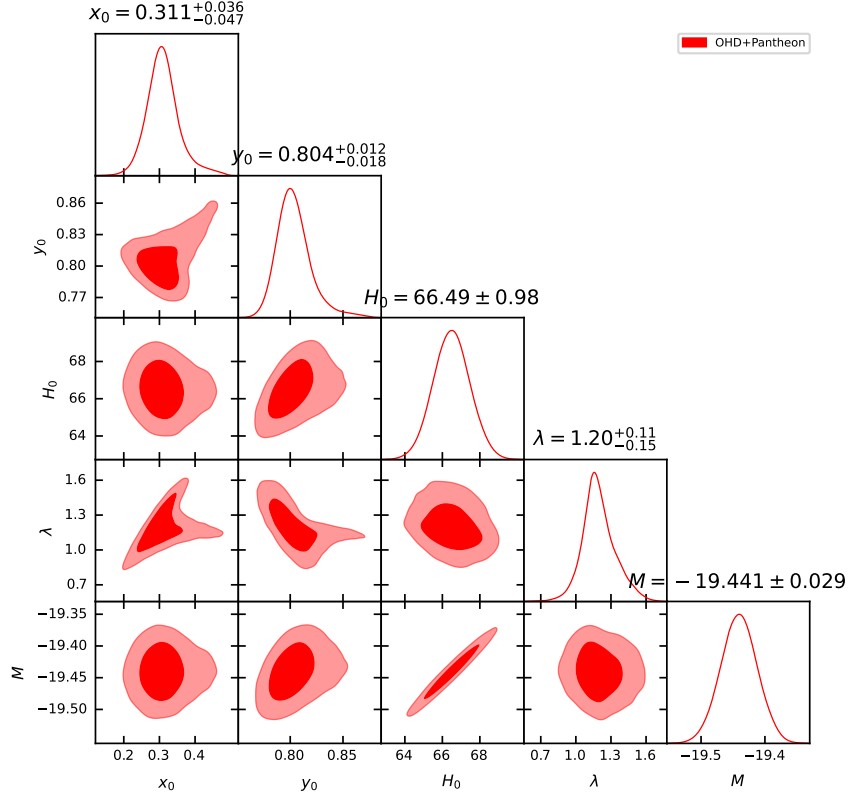


FIG. 6. The Quintessence field is fitted with OHD+Pantheon data.

where M represents the absolute magnitude of the SNe Ia. The luminosity distance d_L in a flat FLRW universe can be calculated as [61],

$$d_L(z) = c(1+z) \int_0^z \frac{dz'}{H(z')}, \quad (4.5)$$

where c is the speed of light in vacuum expressed in the km/s unit. For the SNe Ia, we compute the χ^2 using the expression,

$$\chi_{\text{SNe Ia}}^2 = \Delta \vec{D}^T C_{\text{stat+syst}}^{-1} \Delta \vec{D}, \quad (4.6)$$

where $C_{\text{stat+syst}} = C_{\text{stat}} + C_{\text{syst}}$ is the combined covariance matrix of systematic and statistical uncertainties and \vec{D} is the vector of 1701 SNe Ia distance modulus calculated as

$$\Delta \vec{D} = \mu(z_i) - \mu_{\text{th}}(z_i, H_0, \Omega_{m_0}, M, y_0). \quad (4.7)$$

Here, $\mu(z_i) = m(z_i) - M$ is the distance modulus of SNe Ia. The best fit values of the model parameters are those that minimize the total χ^2 ,

$$\chi_{\text{total}}^2 = \chi_{\text{OHD}}^2 + \chi_{\text{SNe Ia}}^2 \quad (4.8)$$

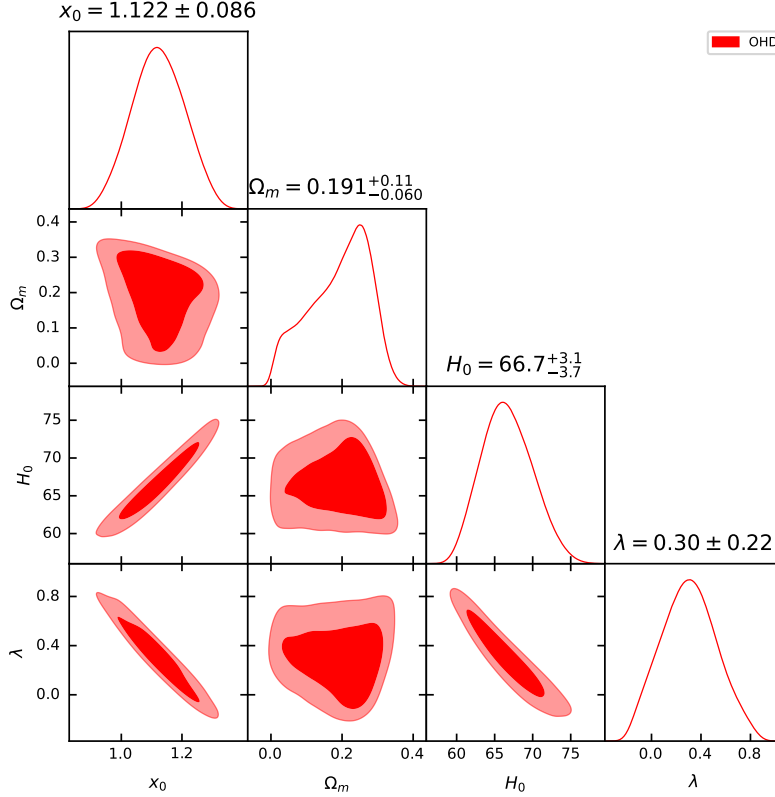


FIG. 7. The k -essence field is fitted with OHD data.

In order to obtain the 1D and 2D posterior probability distribution of the model parameters, we marginalize over the parameters except the parameters under consideration. The information criteria such as Akaike Information Criterion (AIC) [62] and Bayesian Information Criterion (BIC) [63] are used to compare the evidence of Quintessence or k -essence models over the Λ CDM model. The AIC and BIC are defined as [58],

$$\text{AIC} = -2 \ln \mathcal{L}_{\max} + 2k, \quad (4.9)$$

$$\text{BIC} = -2 \ln \mathcal{L}_{\max} + k \ln N \quad (4.10)$$

where k is the number of independent parameters present in the model and N represent the total number of data points and \mathcal{L}_{\max} represents the maximum likelihood. Performing parameter inference involve careful selection of priors for the model parameters. We use flat prior for all the model parameters and dynamical variables summarized in Tab. [III].

We utilized a well tested and openly accessible Python implementation of the affine-invariant ensemble sampler for Markov Chain Monte Carlo (MCMC), as proposed by Goodman and Weare, known as emcee for the Bayesian analysis. More comprehensive information about emcee and its implementation can be found in ref. [64]. The best-fit values of the model parameters are summarized in Tab. [III]. Our analysis shows that both the quintessence and the k -essence models predict $H_0 \sim 67$ close to the value obtained by Planck2018 collaboration assuming the Λ CDM model. However, the value of Ω_{m_0} obtained for the k -essence

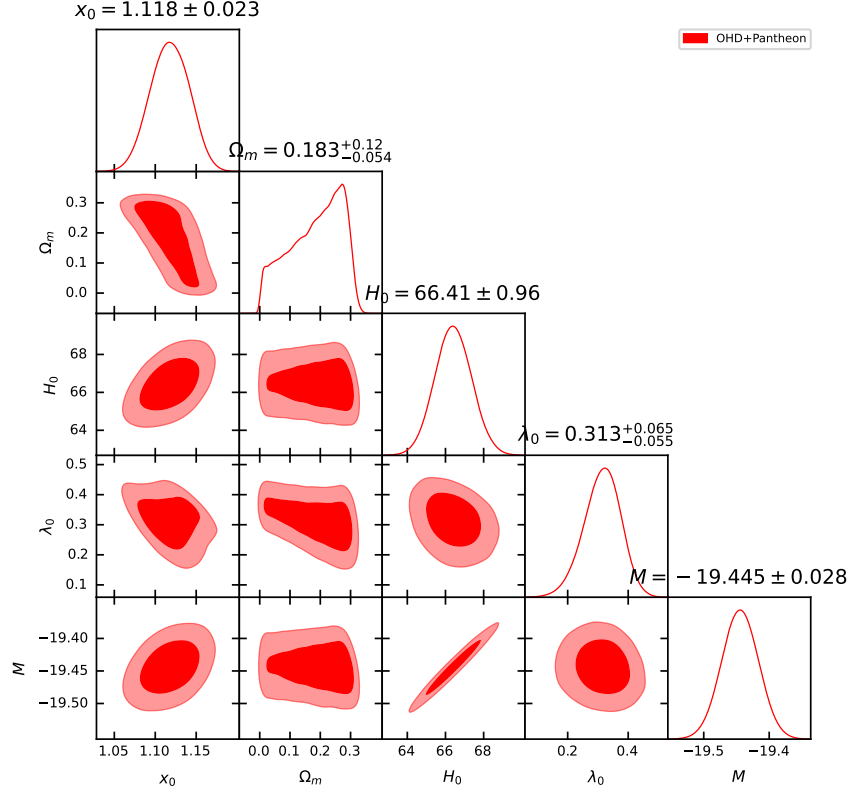


FIG. 8. The k -essence field is fitted with OHD+Pantheon data.

model is slightly less than the standard model prediction for both datasets. The evolution of density parameters corresponding to matter and field for Quintessence and k -essence models are shown in Figs. [10a, 10b]. The Fig.[9], shows the comparison between the apparent magnitude predicted by the Quintessence, the k -essence and the Λ CDM models. It is evident from the figure that all these models predict almost similar $m(z)$ for the best-fit model parameters and consequently showing almost similar fit for the joint analysis. The model selection based on AIC and BIC shows that k -essence model gives slightly better fit to the data as compared to the Quintessence model while the evidence of these models against the Λ CDM model is weak.

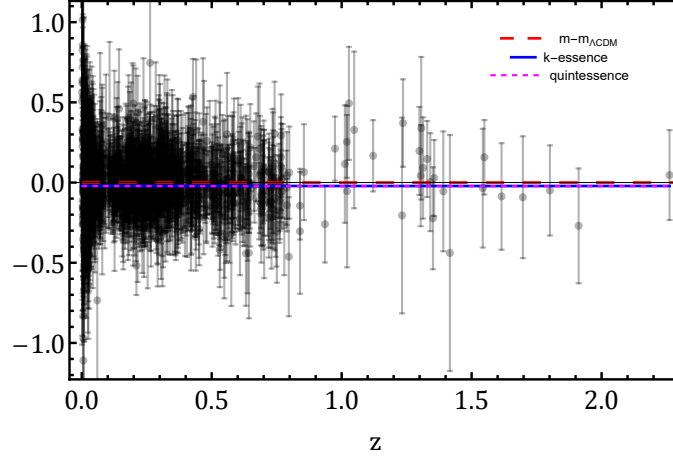


FIG. 9. The residue of $m_{\Lambda\text{CDM}} - m_{k\text{-essence}}$ is plotted in blue, while $m_{\Lambda\text{CDM}} - m_{\text{quintessence}}$ is shown in dotted pink. These are compared with the data points $\Delta m = m_{\text{Data}} - m_{\Lambda\text{CDM}}$. The red dashed line represents $\Delta m = m_{\Lambda\text{CDM}} - m_{\Lambda\text{CDM}} = 0$ (the base line). The comparison shows that both the quintessence and k -essence models exhibit behavior similar to the ΛCDM model. All the lines are very near to each other and so it is difficult to differentiate the colors.

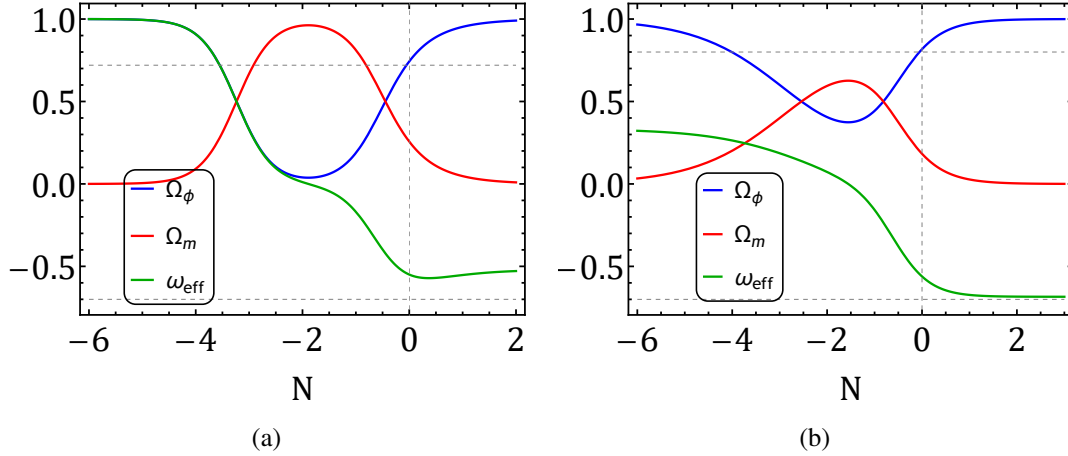


FIG. 10. Evolution of the (a) quintessence and (b) k -essence field corresponding to the best fit values of model parameters obtained from OHD+Pantheon dataset.

Before we end this section we want to opine on the pure kinetic k -essence models, which are thought to be simpler to handle as there are no dynamic potential terms and where the Lagrangian density of the k -essence field is purely a function of X . In these models V is a constant parameter. Such a case is discussed in ref. [36], where the author assumes that the Lagrangian of the k -essence field has an extrema at some point $X = X_0$. It is seen that if one Taylor expands the Lagrangian at $X = X_0$ then one obtains a theory where the energy density

of the k -essence field near X_0 can be represented as a sum of two separate terms. One of these terms can be interpreted to be coming from a dark energy like component and the other term scales with the scale-factor as a^{-3} , specifying a dark matter like component. Pure kinetic k -essence fields can in a certain way unify dark matter and dark energy sectors. The resultant theory has some parameters whose values require to be ascertained by observational data. We see that with our present sets of data it is practically impossible to give any bound on the parameters appearing in the theory. Although a k -essence sector with a non trivial potential can be tackled by our method and we can properly give bounds on various parameters and initial conditions appearing in the theory, it is practically impossible to do such an analysis with a less complicated model. One of the reasons why this happens is perhaps related to the high level of generality of the problem discussed in ref. [36]. This theory is very general in nature and does not specify any particular form of the Lagrangian of the purely kinetic k -essence. Due to this general feature the energy density of the field near the extrema can be expressed in terms of six constants (V_0 , X_0 , F_0 , F_2 , a_1 and ϵ_1). It becomes difficult to put reasonable bounds on all these six parameters using the present set of observational data. As we do not get any positive result for this case we do not present any more detail about this theory here. Readers who want to get a feeling of the difficulty one faces, if one wants to compare it with data, can consult Appendix A where the problem is briefly discussed.

V. CONCLUSION

In this study, we analyzed the quintessence and scalar field models with exponential and inverse square law potentials respectively and compared the theoretical predictions with the Λ CDM model using the observational probes consisting of pantheon+ compilation of Type Ia supernovae (SNIa) and Observational Hubble data (OHD). We employed Markov Chain Monte Carlo (MCMC) method for the parameter inference. Our analysis demonstrated that quintessence and k -essence models are successful in explaining the late time acceleration of the universe. Very few work along this lines, using k -essence have ever been done before. Based on the best values obtained from the joint (OHD+Pantheon) analysis, we observe that the evolution of Ω_m in the presence of the k -essence field takes slightly lower value than in the quintessence-dominated scalar field, as shown in Figs. [10a, 10b].

We see that in the quintessence-dominated field, during the past epoch, the matter density dominates over the field density, and the corresponding effective equation of state becomes zero, signifying the matter-dominated epoch. However, for the k -essence-dominated field, although the matter density dominates, both the field and fluid densities in the past epoch are non-zero and the corresponding effective EoS vanishes, demonstrating that the field may itself behave like some form of matter which produces non-accelerating expansion. Due to this behavior, it can be seen from the evolution plot that in the current epoch, field density is nearly 80%, while the matter density is around 20%. In all of our work we have used the matter part to be composed of a pressure-less fluid. Apart from the distinct density evolution for both fields, the evolution of the effective equation of state (EoS) produces similar values, yet distinct from the Λ CDM model at the current epoch. This is our central result. However, for the quintessence field, the effective equation of state appears to stabilize at -0.50 in the far future, while for the k -essence field, the effective equation of state converges to -0.52 .

The value of H_0 obtained by the quintessence and k -essence models are in close agreement with the value reported by Planck2018 mission assuming the Λ CDM model. The crucial difference between these models can only be observed with high redshift data such as CMB. According to Akaike and Bayesian information criteria for model selection, the evidence of Λ CDM model is slightly higher than the Quintessence and k -essence scenario.

We have also pointed out that the simplest theory of k -essence, only kinetically driven, which can combine both dark matter and dark energy in a combined way cannot be constrained via the observational tools at our hand. The number of parameters in this case make it very difficult for data analysis. In this paper we primarily focused on models where the scalar field sector was not directly coupled to the fluid sector via any non-minimal coupling. It will be interesting to see how non-minimal coupling in the dark sector modifies the results.

Appendix A: A note on pure kinetic k -essence

In ref. [36], the author demonstrated that the k -essence field with a constant potential can unify the dark matter and dark energy phases. In this case, the pure k -essence Lagrangian becomes:

$$P(\phi, X) = V_0 F(X), \quad (\text{A1})$$

where $P(\phi, X)$ denotes the pressure of the k -essence field and V_0 is the constant potential. In the present case we do not assume any specific form of $F(X)$, the only relevant assumption is that $F(X)$ has an extremum at $X = X_0$. In the aforementioned reference it was shown that if such an extremum exists it will be stable under small perturbations around X_0 . In ref. [36] it was shown that the Taylor series expansion of $F(X)$ near its extremum X_0 becomes:

$$F(X) = F_0 + F_2(X - X_0)^2, \quad (\text{A2})$$

where F_0 and F_2 are constants. The corresponding energy density becomes:

$$\rho = V_0 \left(-F_0 + 4F_2 X_0^2 \epsilon_1 (a/a_1)^{-3} \right), \quad (\text{A3})$$

where a_1 is an integration constant with $\epsilon_1 \ll 1$. To constrain the model parameters against the data, we express the Friedmann equation as:

$$3H^2 = \kappa^2 V_0 \left(-F_0 + 4F_2 X_0^2 \epsilon_1 (a/a_1)^{-3} \right). \quad (\text{A4})$$

Rewriting this equation in terms of the redshift z :

$$H(z) = H_0 \sqrt{\Omega_{F_0} - 4 \frac{F_2}{F_0} \Omega_{F_0} X_0^2 \epsilon_1 a_1^3 (1+z)^3}, \quad (\text{A5})$$

where $\Omega_{F_0} = \frac{-F_0 \kappa^2 V_0}{3H_0^2}$. We can express other constants in terms of Ω_{F_0} by using the condition that at $z = 0$, $H = H_0$:

$$\epsilon_1 = \frac{F_0}{4F_2 X_0^2 a_1^3} \left(1 - \frac{1}{\Omega_{F_0}} \right). \quad (\text{A6})$$

Inserting this into the above equation results in:

$$H(z) = H_0 \sqrt{\Omega_{F_0} - \Omega_{F_0}(1 - 1/\Omega_{F_0})(1 + z)^3}, \quad (\text{A7})$$

which takes the same form as Λ CDM. From this, we see that it is not possible to constrain all the model parameters of the kinetic k-essence. One can only obtain constraints on Ω_{F_0} , and from this information, one can at best estimate the range of some parameters by assuming certain values for other parameters. Here, we will get the same value for Ω_{F_0} as Ω_{Λ_0} as determined in Tab. III.

-
- [1] S. Perlmutter *et al.* (Supernova Cosmology Project), Measurements of Ω and Λ from 42 high redshift supernovae, *Astrophys. J.* **517**, 565 (1999), [arXiv:astro-ph/9812133](#).
 - [2] A. G. Riess *et al.* (Supernova Search Team), Observational evidence from supernovae for an accelerating universe and a cosmological constant, *Astron. J.* **116**, 1009 (1998), [arXiv:astro-ph/9805201](#).
 - [3] D. N. Spergel *et al.* (WMAP), First year Wilkinson Microwave Anisotropy Probe (WMAP) observations: Determination of cosmological parameters, *Astrophys. J. Suppl.* **148**, 175 (2003), [arXiv:astro-ph/0302209](#).
 - [4] B. D. Sherwin *et al.*, Evidence for dark energy from the cosmic microwave background alone using the Atacama Cosmology Telescope lensing measurements, *Phys. Rev. Lett.* **107**, 021302 (2011), [arXiv:1105.0419 \[astro-ph.CO\]](#).
 - [5] E. L. Wright, Constraints on Dark Energy from Supernovae, Gamma Ray Bursts, Acoustic Oscillations, Nucleosynthesis and Large Scale Structure and the Hubble constant, *Astrophys. J.* **664**, 633 (2007), [arXiv:astro-ph/0701584](#).
 - [6] J. Kwan *et al.* (DES), Cosmology from large-scale galaxy clustering and galaxy–galaxy lensing with Dark Energy Survey Science Verification data, *Mon. Not. Roy. Astron. Soc.* **464**, 4045 (2017), [arXiv:1604.07871 \[astro-ph.CO\]](#).
 - [7] T. M. C. Abbott *et al.* (DES), Dark Energy Survey Year 3 results: A 2.7% measurement of baryon acoustic oscillation distance scale at redshift 0.835, *Phys. Rev. D* **105**, 043512 (2022), [arXiv:2107.04646 \[astro-ph.CO\]](#).
 - [8] D. J. Eisenstein *et al.* (SDSS), Detection of the Baryon Acoustic Peak in the Large-Scale Correlation Function of SDSS Luminous Red Galaxies, *Astrophys. J.* **633**, 560 (2005), [arXiv:astro-ph/0501171](#).
 - [9] E. J. Copeland, M. Sami, and S. Tsujikawa, Dynamics of dark energy, *Int. J. Mod. Phys. D* **15**, 1753 (2006), [arXiv:hep-th/0603057](#).
 - [10] S. Weinberg, The Cosmological Constant Problem, *Rev. Mod. Phys.* **61**, 1 (1989).
 - [11] S. E. Rugh and H. Zinkernagel, The Quantum vacuum and the cosmological constant problem, *Stud. Hist. Phil. Sci. B* **33**, 663 (2002), [arXiv:hep-th/0012253](#).
 - [12] T. Padmanabhan, Cosmological constant: The Weight of the vacuum, *Phys. Rept.* **380**, 235 (2003), [arXiv:hep-th/0212290](#).
 - [13] S. M. Carroll, W. H. Press, and E. L. Turner, The Cosmological constant, *Ann. Rev. Astron. Astrophys.* **30**, 499 (1992).

- [14] G. R. Bengochea, G. León, E. Okon, and D. Sudarsky, Can the quantum vacuum fluctuations really solve the cosmological constant problem?, *Eur. Phys. J. C* **80**, 18 (2020), [arXiv:1906.05406 \[gr-qc\]](#).
- [15] K. Kohri and H. Matsui, Cosmological Constant Problem and Renormalized Vacuum Energy Density in Curved Background, *JCAP* **06**, 006, [arXiv:1612.08818 \[hep-th\]](#).
- [16] M. López-Corredoira, Tests and problems of the standard model in Cosmology, *Found. Phys.* **47**, 711 (2017), [arXiv:1701.08720 \[astro-ph.CO\]](#).
- [17] N. Aghanim, Y. Akrami, M. Ashdown, J. Aumont, C. Baccigalupi, M. Ballardini, A. J. Banday, R. Barreiro, N. Bartolo, S. Basak, *et al.*, *A&A* **641**, A6 (2020).
- [18] A. G. Riess, S. Casertano, W. Yuan, J. B. Bowers, L. Macri, J. C. Zinn, and D. Scolnic, *Astrophys. J. Lett.* **908**, L6 (2021).
- [19] P. J. E. Peebles and B. Ratra, The Cosmological Constant and Dark Energy, *Rev. Mod. Phys.* **75**, 559 (2003), [arXiv:astro-ph/0207347](#).
- [20] T. Nishioka and Y. Fujii, Inflation and the decaying cosmological constant, *Phys. Rev. D* **45**, 2140 (1992).
- [21] P. G. Ferreira and M. Joyce, Cosmology with a primordial scaling field, *Phys. Rev. D* **58**, 023503 (1998), [arXiv:astro-ph/9711102](#).
- [22] I. Zlatev, L.-M. Wang, and P. J. Steinhardt, Quintessence, cosmic coincidence, and the cosmological constant, *Phys. Rev. Lett.* **82**, 896 (1999), [arXiv:astro-ph/9807002](#).
- [23] E. J. Copeland, A. R. Liddle, and D. Wands, Exponential potentials and cosmological scaling solutions, *Phys. Rev. D* **57**, 4686 (1998), [arXiv:gr-qc/9711068](#).
- [24] A. Hebecker and C. Wetterich, Quintessential adjustment of the cosmological constant, *Phys. Rev. Lett.* **85**, 3339 (2000), [arXiv:hep-ph/0003287](#).
- [25] A. Hebecker and C. Wetterich, Natural quintessence?, *Phys. Lett. B* **497**, 281 (2001), [arXiv:hep-ph/0008205](#).
- [26] N. Roy, S. Goswami, and S. Das, Quintessence or phantom: Study of scalar field dark energy models through a general parametrization of the Hubble parameter, *Phys. Dark Univ.* **36**, 101037 (2022), [arXiv:2201.09306 \[astro-ph.CO\]](#).
- [27] S. Hussain, A. Chatterjee, and K. Bhattacharya, Dynamical stability in models where dark matter and dark energy are nonminimally coupled to curvature, *Phys. Rev. D* **108**, 103502 (2023), [arXiv:2305.19062 \[gr-qc\]](#).
- [28] S. Das, S. Hussain, D. Nandi, R. O. Ramos, and R. Silva, Stability analysis of warm quintessential dark energy model, *Phys. Rev. D* **108**, 083517 (2023), [arXiv:2306.09369 \[gr-qc\]](#).
- [29] C. Armendariz-Picon, V. F. Mukhanov, and P. J. Steinhardt, A Dynamical solution to the problem of a small cosmological constant and late time cosmic acceleration, *Phys. Rev. Lett.* **85**, 4438 (2000), [arXiv:astro-ph/0004134](#).
- [30] C. Armendariz-Picon, V. F. Mukhanov, and P. J. Steinhardt, Essentials of k essence, *Phys. Rev. D* **63**, 103510 (2001), [arXiv:astro-ph/0006373](#).
- [31] T. Chiba, T. Okabe, and M. Yamaguchi, Kinetically driven quintessence, *Phys. Rev. D* **62**, 023511 (2000), [arXiv:astro-ph/9912463](#).
- [32] W. Fang, H. Tu, Y. Li, J. Huang, and C. Shu, Full Investigation on the Dynamics of Power-Law Kinetic Quintessence, *Phys. Rev. D* **89**, 123514 (2014), [arXiv:1406.0128 \[gr-qc\]](#).

- [33] C. Armendariz-Picon, T. Damour, and V. F. Mukhanov, k - inflation, *Phys. Lett. B* **458**, 209 (1999), [arXiv:hep-th/9904075](#).
- [34] C. Armendariz-Picon and E. A. Lim, Haloes of k-essence, *JCAP* **08**, 007, [arXiv:astro-ph/0505207](#).
- [35] N. Arkani-Hamed, H.-C. Cheng, M. A. Luty, and S. Mukohyama, Ghost condensation and a consistent infrared modification of gravity, *JHEP* **05**, 074, [arXiv:hep-th/0312099](#).
- [36] R. J. Scherrer, Purely kinetic k-essence as unified dark matter, *Phys. Rev. Lett.* **93**, 011301 (2004), [arXiv:astro-ph/0402316](#).
- [37] A. Chatterjee, S. Hussain, and K. Bhattacharya, Dynamical stability of the k-essence field interacting nonminimally with a perfect fluid, *Phys. Rev. D* **104**, 103505 (2021), [arXiv:2105.00361 \[gr-qc\]](#).
- [38] S. Hussain, A. Chatterjee, and K. Bhattacharya, Ghost Condensates and Pure Kinetic k-Essence Condensates in the Presence of Field–Fluid Non-Minimal Coupling in the Dark Sector, *Universe* **9**, 65 (2023), [arXiv:2203.10607 \[gr-qc\]](#).
- [39] K. Bhattacharya, A. Chatterjee, and S. Hussain, Dynamical stability in presence of non-minimal derivative dependent coupling of k-essence field with a relativistic fluid, *Eur. Phys. J. C* **83**, 488 (2023), [arXiv:2206.12398 \[gr-qc\]](#).
- [40] A. A. Coley, *Dynamical systems and cosmology* (Kluwer, Dordrecht, Netherlands, 2003).
- [41] A. D. Rendall, Cosmological models and center manifold theory, *Gen. Rel. Grav.* **34**, 1277 (2002), [arXiv:gr-qc/0112040](#).
- [42] C. G. Boehmer, N. Chan, and R. Lazkoz, Dynamics of dark energy models and centre manifolds, *Phys. Lett. B* **714**, 11 (2012), [arXiv:1111.6247 \[gr-qc\]](#).
- [43] J. Dutta, W. Khylllep, and N. Tamanini, Dark energy with a gradient coupling to the dark matter fluid: cosmological dynamics and structure formation, *JCAP* **01**, 038, [arXiv:1707.09246 \[gr-qc\]](#).
- [44] D. L. Blackmore, V. H. Samoylenko, *et al.*, *Nonlinear dynamical systems of mathematical physics: spectral and symplectic integrability analysis* (World Scientific, 2011).
- [45] M. Bouhmadi-López, J. a. Marto, J. a. Morais, and C. M. Silva, Cosmic infinity: A dynamical system approach, *JCAP* **03**, 042, [arXiv:1611.03100 \[gr-qc\]](#).
- [46] U. Elias and H. Gingold, Critical points at infinity and blow up of solutions of autonomous polynomial differential systems via compactification, *Journal of mathematical analysis and applications* **318**, 305 (2006).
- [47] S. Bahamonde, C. G. Böhmmer, S. Carloni, E. J. Copeland, W. Fang, and N. Tamanini, Dynamical systems applied to cosmology: dark energy and modified gravity, *Phys. Rept.* **775-777**, 1 (2018), [arXiv:1712.03107 \[gr-qc\]](#).
- [48] N. Roy, A. X. Gonzalez-Morales, and L. A. Urena-Lopez, New general parametrization of quintessence fields and its observational constraints, *Phys. Rev. D* **98**, 063530 (2018), [arXiv:1803.09204 \[gr-qc\]](#).
- [49] L. A. Ureña López and N. Roy, Generalized tracker quintessence models for dark energy, *Phys. Rev. D* **102**, 063510 (2020), [arXiv:2007.08873 \[astro-ph.CO\]](#).
- [50] N. Roy and K. Bamba, Arbitrariness of potentials in interacting quintessence models, *Phys. Rev. D* **99**, 123520 (2019), [arXiv:1811.03234 \[astro-ph.CO\]](#).
- [51] R.-J. Yang and X.-T. Gao, Observational constraints on purely kinetic k-essence dark energy models, *Chin. Phys. Lett.* **26**, 089501 (2009).

- [52] B. R. Dinda and N. Banerjee, Constraints on the speed of sound in the k-essence model of dark energy, *Eur. Phys. J. C* **84**, 177 (2024), [arXiv:2309.10538 \[astro-ph.CO\]](#).
- [53] S. Cao, T.-J. Zhang, X. Wang, and T. Zhang, Cosmological Constraints on the Coupling Model from Observational Hubble Parameter and Baryon Acoustic Oscillation Measurements, *Universe* **7**, 57 (2021), [arXiv:2103.03670 \[astro-ph.CO\]](#).
- [54] D. M. Scolnic *et al.* (Pan-STARRS1), The Complete Light-curve Sample of Spectroscopically Confirmed SNe Ia from Pan-STARRS1 and Cosmological Constraints from the Combined Pantheon Sample, *Astrophys. J.* **859**, 101 (2018), [arXiv:1710.00845 \[astro-ph.CO\]](#).
- [55] A. Bonilla Rivera and J. E. García-Farieta, Exploring the Dark Universe: constraints on dynamical Dark Energy models from CMB, BAO and growth rate measurements, *Int. J. Mod. Phys. D* **28**, 1950118 (2019), [arXiv:1605.01984 \[astro-ph.CO\]](#).
- [56] H. Amirhashchi and S. Amirhashchi, Constraining Bianchi Type I Universe With Type Ia Supernova and $H(z)$ Data, *Phys. Dark Univ.* **29**, 100557 (2020), [arXiv:1802.04251 \[astro-ph.CO\]](#).
- [57] M. Moresco, Raising the bar: new constraints on the Hubble parameter with cosmic chronometers at $z \sim 2$, *Mon. Not. Roy. Astron. Soc.* **450**, L16 (2015), [arXiv:1503.01116 \[astro-ph.CO\]](#).
- [58] R. Trotta, Bayes in the sky: Bayesian inference and model selection in cosmology, *Contemp. Phys.* **49**, 71 (2008), [arXiv:0803.4089 \[astro-ph\]](#).
- [59] S. N and T. K. Mathew, Running vacuum model versus Λ CDM – a Bayesian analysis, *Mon. Not. Roy. Astron. Soc.* **510**, 5553 (2022), [arXiv:2105.03084 \[gr-qc\]](#).
- [60] L. E. Padilla, L. O. Tellez, L. A. Escamilla, and J. A. Vazquez, Cosmological Parameter Inference with Bayesian Statistics, *Universe* **7**, 213 (2021), [arXiv:1903.11127 \[astro-ph.CO\]](#).
- [61] D. Brout *et al.*, The Pantheon+ Analysis: Cosmological Constraints, *Astrophys. J.* **938**, 110 (2022), [arXiv:2202.04077 \[astro-ph.CO\]](#).
- [62] H. Akaike, A new look at the statistical model identification, *IEEE Transactions on Automatic Control* **19**, 716 (1974).
- [63] G. Schwarz, Estimating the dimension of a model, *The Annals of Statistics* **6**, 461 (1978).
- [64] D. Foreman-Mackey, D. W. Hogg, D. Lang, and J. Goodman, emcee: The mcmc hammer, *Publications of the Astronomical Society of the Pacific* **125**, 306–312 (2013).